energies

MDPI

Article

Control Research on Active Pitch Control System for Horizontal-Axis Tidal-Current Turbine Generator

Fuli Zhang [1,2], Wanqiang Zhu [1,2,*], Shuai Zu [1,2], Xueming Zhang [1,2], Jianmei Chen [1,2], Baigong Wu [3] and Jipeng Huang [1,2]

[1] School of Physics, Northeast Normal University, 5268 Renmin Street, Changchun 130024, China; zhangfl950@nenu.edu.cn (F.Z.)
[2] Jilin Provincial Key Laboratory of Advanced Energy Development and Application Innovation, 5268 Renmin Street, Changchun 130024, China
[3] Institute of Marine Equipment, Jiangsu University of Science and Technology, Zhenjiang 212000, China
* Correspondence: zhuwq773@nenu.edu.cn

Abstract: Tidal energy, as a sustainable and environmentally friendly energy source, has attracted widespread attention in recent years. The technology of blade active pitch control is the key technology to cope with tidal velocity change and improve the stability and efficiency of horizontal-axis tidal generator sets. When solving the problem of speed variation, the core algorithm is the key to ensuring stable operation and improving the efficiency of power generation. When traditional PID is used to manage complex systems, the controller faces the challenge of complex parameter tuning and insufficient robustness. The application of a particle swarm optimization (PSO)–PID controller and fuzzy PID controller in the independent interval system of tidal generator sets is introduced for the first time in this paper. This paper presents a comparative study of unified pitch control and independent pitch control (using electric pitch control) for a three-rotor tidal generator with a rated capacity of 300 kw and a blade radius of 8.5 m. Simulation was carried out on the MATLAB/Simulink (2023a) platform to evaluate the performance of the two controllers under different flow rates and interference conditions. The results show that the PSO-PID controller has significant advantages in reducing overshoot, speeding up response times, and improving power generation efficiency. At the same time, the PSO-PID controller also shows superior performance in pitch angle adjustment frequency and generator output power and realizes timely and effective system stability control.

Keywords: tidal energy; water turbines; PSO-PID; fuzzy PID; active pitch control

check for updates

Academic Editor: Frede Blaabjerg

Received: 2 December 2024
Revised: 24 January 2025
Accepted: 26 January 2025
Published: 7 February 2025

Citation: Zhang, F.; Zhu, W.; Zu, S.; Zhang, X.; Chen, J.; Wu, B.; Huang, J. Control Research on Active Pitch Control System for Horizontal-Axis Tidal-Current Turbine Generator. *Energies* **2025**, *18*, 764. https://doi.org/10.3390/en18040764

Copyright: © 2025 by the authors. Licensee MDPI, Basel, Switzerland. This article is an open access article distributed under the terms and conditions of the Creative Commons Attribution (CC BY) license (https://creativecommons.org/licenses/by/4.0/).

1. Introduction

Amidst the continuous transformation of the global energy structure and the formidable challenges brought about by climate change [1], the vast energy potential and sustainability of ocean tidal currents have increasingly come into the spotlight. Tidal turbines, functioning as crucial apparatuses for the conversion of ocean tidal energy into electrical energy, generally comprise blades, rotors, transmission systems, generators, and support structures. The blades are meticulously designed to capture tidal energy with high efficiency. When under the influence of water flow, the blades set the rotor in motion, transferring mechanical energy to the generator via the transmission system, where it is then converted into electrical output (as depicted in Figure 1).

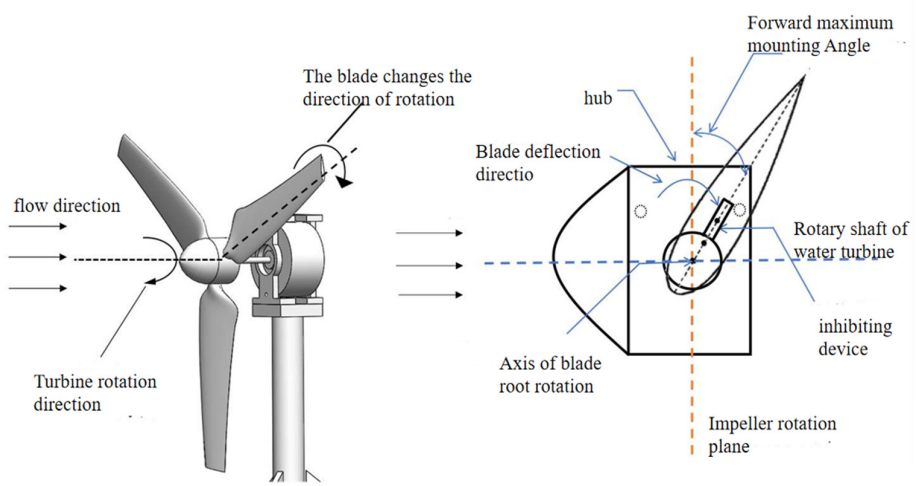

Figure 1. Integral hydraulic turbine.

The depth and velocity of tidal currents pose substantial challenges to large-scale tidal current power generation devices. Specifically, variations in flow depth can alter the gradient of flow velocity, and the resulting depth-dependent changes in flow velocity have a notable effect on the efficiency and loading of tidal current turbines, consequently influencing blade stability. These variations may give rise to problems such as blade vibration and fatigue. At present, research on tidal current generators predominantly centers around unified pitch control, while independent pitch control is mainly applied to wind turbines. To enhance the operational stability and efficiency of tidal stream generator sets, active pitch control has emerged as one of the core technologies in the control system of tidal stream generators [2].

Different pitch control strategies have their advantages and disadvantages in the study of active pitch control systems based on horizontal-axis tidal-flow-energy turbine blades [3]. The following summary table compares the two main control strategies of unified pitch control and independent pitch control in detail and the challenges they faced (Table 1).

Table 1. Different tilt control strategies and their challenges.

Pitch Control Strategy	Advantage	Challenge
Unified pitch control	Simple control, low cost, adjustable overall power to improve efficiency	It is difficult to accurately adapt the water flow of each blade, the response to the change of water flow is weak, and the failure of a single blade affects the whole system
Independent variable pitch control	It can accurately adjust the paddle, improve the efficiency, stabilize the unit, reduce the blade load, and adapt to complex water flow	The algorithm is complex, hardware and maintenance costs are high, the sensor execution fault has great influence, and the communication requirement is high—communication problems may affect the control effect

The research and public literature regarding active pitch control technology in tidal stream generator sets is scarce. The independent variable pitch load control strategy based on fuzzy PID parameter self-tuning was studied by Lin Yonggang's team from Zhejiang University for the 120 kW horizontal-axis ocean-current generator set, aiming to reduce the asymmetric load caused by ocean current turbulence and shear action in the impeller plane. Through the establishment of the blade rotation coordinate system and the

impeller fixed coordinate system, the blade force was converted to pitch moment and yaw moment and the blade root bending moment was transformed to the d-q coordinate system. However, the Coleman transformation and its inverse require significant calculations. For real-time control systems, this can increase the computational load, particularly during high-frequency load changes, potentially causing response delays. Controlling the root bending moment by the adaptive gain method under the flow velocity shear of the tidal power generator set has been investigated in the literature [4], but the algorithm is rather complex and only numerical simulation has been carried out under low shear load. Although there are numerous similarities in principle and structure between the horizontal-axis tidal-stream generator set and the wind turbine set, the variable pitch mechanisms of the two sets are significantly different. The hub space of the tidal stream and the generator set are compact, with an extremely stringent sealing requirement, further complicated by the marine environment's intricacies, thus presenting additional challenges in designing a variable pitch system [5]. The vertical axis of the ocean-current power generation device at University College London, UK (University College London), employs hydraulic pitch. The hydraulic variable rotor has a compact structure and large driving torque, which is suitable for working conditions with limited hub space and large load torque. Nevertheless, the maintenance cost of the hydraulic system is high and there is a risk of environmental pollution caused by fuel leakage [6]. In contrast, the 300 kW horizontal-axial current power generation unit from MCT in the UK and Norway adopts an electrical variable pitch system. Electric variable pitch has greater requirements on hub space and is vulnerable to impact, but its response speed is fast and efficiency is high, making it more suitable for high-power generator sets [7,8]. Therefore, in this study, the electric variable pitch mode was selected to achieve the active variable pitch control of the new horizontal-axis self-variable pitch tidal power generator set.

In the selection of algorithms, PID control is widely employed in the field of industrial control due to its simplicity, effectiveness, and proven track record in various industrial applications. However, the traditional PID controller's performance becomes constrained in complex operating scenarios, making it challenging to fulfill the high-precision demands of variable pitch control. Therefore, in recent years, a variety of optimization algorithms and intelligent control technologies have been introduced into the power flow control system. The particle swarm optimization (PSO) algorithm and fuzzy PID control are two representative methods. The particle swarm optimization (PSO) algorithm demonstrates excellent searching ability and fast convergence speeds in multi-objective optimization problems, which makes it a powerful tool for solving complex system optimization problems [9]. Additionally, the fuzzy control algorithm is frequently used in research on the pitch control of power flow generators because of its strong robustness [10].

By drawing from these two algorithms, this study proposes an active electronically controlled pitch control algorithm for self-variable pitch tidal power turbines and builds a highly comprehensive dynamic model encompassing hydraulic power, mechanical power, and electrical energy conversion, which enhances energy conversion efficiency and improves the operational stability of the generator set under variable working conditions [11]. Through a comparative study of simulation experiments of the unified pitch change and independent pitch change of the turbine, the influence of tidal flow speed changes and marine environment interference can be mitigated by adjusting the pitch of the blade separately and quickly. Furthermore, by comparing the experimental (simulation) results of conventional control strategies, the proposed algorithm demonstrates significant advantages in terms of power generation efficiency, mechanical loss reduction, and environmental adaptation. The results indicate that PSO can not only effectively improve the power flow conversion

efficiency but also provide a new idea for the control strategy of self-variable pitch power flow turbines, which holds significant practical value and theoretical significance.

For convenience, the meanings of each parameter are shown in Table 2.

Table 2. Meaning of each parameter.

$C_{P(\lambda,\beta)}$	Power coefficient	n_g	Transmission ratio	J_r	Rotor inertia	w_g	Generator speed
$C_{Q(\lambda,\beta)}$	Torque coefficient	R	Rotor radius	k_B	Blade elasticity coefficient	θ_r	Rotor azimuth
$C_{T(\lambda,\beta)}$	Thrust coefficient	T_a	Electric torque	k_s	Blade quality	θ_g	Generator azimuth
d_B	Blade damping coefficient	T_g	Generator torque	m_B	Number of blades	β	Pitch angle
d_S	Torque damping coefficient	T_{gd}	Expected generator torque	ρ	Density of water	θ_s	Twist angle
F_T	Resistance	v	Effective flow rate	T	Time constant	β_d	Desired pitch angle
J_g	Generator inertia	w_r	Rotor speed	T_g	Time constant	T_i	Time constant

2. Modeling of Power Flow Turbine System

A turbine is a mechanical system that converts hydrodynamic power into electrical energy. Therefore, achieving maximum power output while minimizing mechanical load is crucial for the upscaling of equipment [12]. Therefore, the controller is supposed to control both the output power and the output load. The mathematical model of a horizontal-axis three-bladed independent variable-pitch turbine synergistically integrates the mechanical dynamics of the turbine with the electromagnetic dynamics of the generator. To describe the system in detail, it is typically necessary to proceed from three aspects: the mechanical model of the turbine, the electrical model of the generator, and the control system model [13].

2.1. Hydro Turbine System Physical Modeling

Mathematical modeling is performed based on the characteristics of variable pitch control for a three-blade turbine and the geometric features of the blades (Figures 2 and 3). The modeling process encompasses multiple disciplines, including fluid mechanics, mechanical design, and energy conversion. The design presented in this study was informed by data from swept-back blades, as evidenced by the optimization of sludge return pumps with varying sweep angles, which demonstrated improved efficiency and performance. The following sections outline the primary steps and considerations involved in modeling such a turbine.

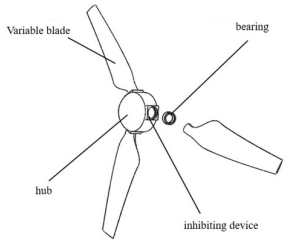

Figure 2. 3D blade diagram.

To simplify the model, the following assumptions could be made:

Considering the complex fluid–structure coupling problem caused by blade deformation, the calculation amount increased dramatically. In the initial stage of studying the basic principle and control strategy design of the tidal flow power generation system, the rigid blade hypothesis could eliminate the disturbance of blade deformation and allow the researchers to focus on the core problem. For example, when designing the active pitch control system, the influence of the control strategy on the system performance could be

intuitively analyzed and the control algorithm could be quickly optimized. The rigid blade hypothesis made the mathematical model derivation more concise, without introducing complex deformation equations, and convenient for theoretical derivation.

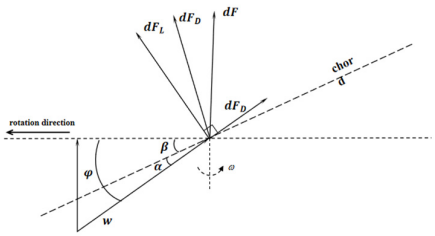

Figure 3. Real picture of blade motion.

The fluid was incompressible and non-viscous. The flow was stable. That is, the velocity and pressure did not change with time. The blade was rigid and did not deform [14].

The main parameters included blade angle θ, blade, radius r, water flow velocity v, water density ρ, and rotational speed ω.

According to the dynamics equation of the turbine, the captured power was expressed as

$$P_i = \frac{1}{2}\rho A C_P(\beta_i, \lambda) v^3 \tag{1}$$

P_i is the output torque of the first i blade, ρ is the water flow density (assumed to be 1025 kg/m^3, A is the swept area of the blade, C_T is the torque coefficient, β_i is the variable blade angle of the blade, λ is the tip speed ratio, and v is the water speed.

The tip velocity ratio was related to the rotational speed and water velocity and defined as $\lambda = \frac{\omega_r R}{v}$, $C_p(\lambda,\ \beta)$, as shown in Formula (17).

The power torque T_a and resistance of the turbine F_T could be expressed as

$$T_a = \frac{1}{2}\rho\pi R^3 \frac{C_P(\lambda,\beta)}{\lambda} v^2 = \frac{1}{2}\rho\pi R^3 C_P(\lambda,\beta) v^2 \tag{2}$$

$$F_T = \frac{1}{2}\rho\pi R^2 C_T(\lambda,\beta) v^2 \tag{3}$$

The electrical characteristics of a three-phase synchronous generator are described by its stator and rotor equations.

The stator voltage equation:

$$v_s = R_s i_s + \frac{d\phi_s}{d_t} \tag{4}$$

Rotor voltage equation:

$$v_f = R_i i_f + \frac{d\phi_f}{dt} \tag{5}$$

Relation between mechanical power and electromagnetic power:

The mechanical power of the water wheel was transferred to the generator through the transmission system, and the balance relationship between the mechanical power and the electromagnetic power was expressed by the torque equation:

$$T_m = T_e + J\frac{d_\omega}{dt} \tag{6}$$

The main task of the control system was to adjust the pitch angle and the excitation current to optimize the power output and stability β_i.

Variable pitch control: The variable pitch angle of each blade.

This was adjusted by a separate controller. A proportional integral differential (PID) controller is usually used to adjust pitch angles to respond to different water speed changes or maximize power output.

The controller equation could be written as

$$\beta_i(t) = K_p e(t) + K_i \int e(t)dt + K_d \frac{de(t)}{dt} \tag{7}$$

By integrating mechanical and electrical models, a state–space model could be formulated to capture the dynamic behavior of the entire system, as detailed in the comprehensive guide on system mechanics-based state–space model construction. For this model, state variables could be defined:

$$\dot{x} = Ax + Bu \tag{8}$$

$$y = Cx + Du \tag{9}$$

The state vector x could be defined as

$$x = \begin{bmatrix} \omega \\ \theta \\ I_S \\ \psi_S \end{bmatrix} \tag{10}$$

The control input u included u_1 and u_2, and u the control input vector was defined as

$$u = \begin{bmatrix} u_1 \\ u_2 \end{bmatrix} \tag{11}$$

The matrix describes the internal coupling relationship between state variables. A was obtained by linearizing the dynamical and electrical equations of the system. We needed to derive the first-order differential equation from the power equation and voltage equation of the turbine and generator and then linearize it and express it in matrix form.

$$A = \begin{bmatrix} \frac{-\left(c_1\omega + c_2\omega^2 + c_4\omega^2 + c_5\omega^3\right)}{J} & 0 & 0 & 0 \\ 0 & 0 & 0 & 0 \\ 0 & 0 & 0 & 0 \\ 0 & 0 & 0 & 0 \end{bmatrix} \tag{12}$$

The matrix represents the influence of the control input on the state of the system, usually acting on the system through the controller B. Control inputs such as pitch angle, control signals, and excitation current control signals affect the state of the system, e.g., u_1 u_2 B. The expression for the matrix could be written as

$$B = \begin{bmatrix} \frac{c_3\lambda^{p_1}\beta_1^{p_2}\beta_2^{p_3}\beta_3^{p_4}\rho A V_t^2/2\omega - c_4\omega^2 - c_5\omega^3}{J} & 0 & 0 & 0 \\ 0 & 1 & 0 & 0 \\ 0 & 0 & 1 & 0 \\ 0 & 0 & 0 & 1 \end{bmatrix} \tag{13}$$

$$C = \begin{bmatrix} 1 & 0 & 0 & 0 \\ 0 & 0 & 0 & c_4\omega^3 + c_5\omega^4 \end{bmatrix} \tag{14}$$

$$D = \begin{bmatrix} 0 & 0 & 0 \\ 0 & 0 & 0 \end{bmatrix} \tag{15}$$

2.2. Fluid Dynamics Model

The fluid dynamics section usually utilizes the Bernoulli equation and the momentum theorem [15].

Kinetic energy conversion: Water flow kinetic energy was converted into the mechanical energy of the turbine during the process in which the fluid worked on the blade. The power P could be expressed as:

$$P = \frac{1}{2} \cdot \rho \cdot A \cdot v^3 \cdot C_P \tag{16}$$

where A is the cross-sectional area of the blade, $A = \pi \cdot r^2$.

C_P is the energy coefficient, which is related to blade design and angle.

$$C_P = (0.44 - 0.0167\beta)\sin\left[\frac{\pi(\lambda - 3)}{15 - 0.3\beta}\right] - 0.00184(\lambda - 3)\beta \tag{17}$$

The resulting curve C_P is shown in in Figure 4 below:

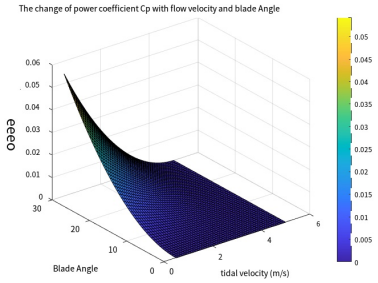

Figure 4. Power coefficient of 300 kw three-blade tidal current turbine generator.

Momentum change: The force generated by the water flow on the blade was calculated using the momentum theorem:

$$F = \rho \cdot Q \cdot \Delta v \tag{18}$$

where Q is the flow rate, $Q = A \cdot v$, and Δv is the change in velocity. The moment T generated by the flow on the blade can be expressed as $T = F \cdot r$. The output power P_O of the turbine is $P_O = T \cdot \omega$. This can be further written as $P_O = F \cdot R \cdot \omega$ η can be expressed as $\eta = \frac{P_O}{P_{in}}$, where P_{in} is the kinetic energy of the fluid and P_O is the actual output power.

Through the above modeling process, the simulation platform was built in Simulink. The hydraulic turbine simulation model is shown in Figure 5:

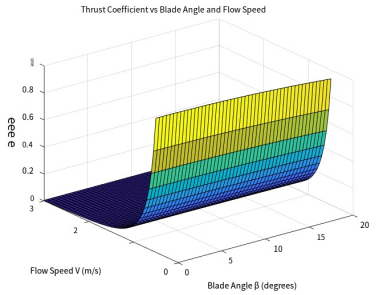

Figure 5. Thrust coefficient of 300 kw three-blade tidal current turbine.

The essence of this model revolves around calculating the hydrodynamic torque of the blade, integrating the electrical equation, and optimizing the control of pitch angle and excitation current (Figure 6).

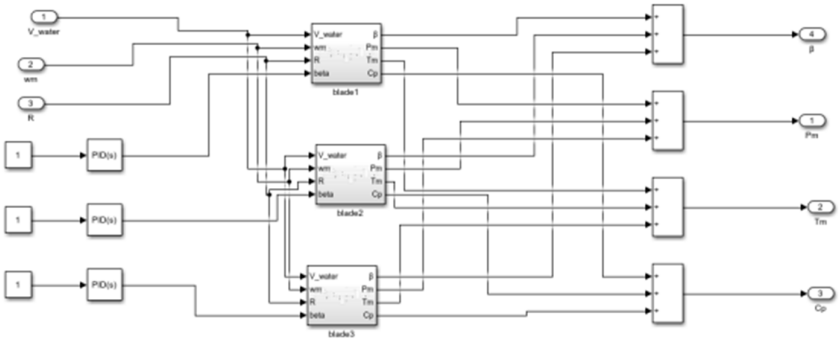

Figure 6. Thrust coefficient of 300 kw three-blade tidal current turbine.

3. Design of Independent Pitch Control System

The design of an independent pitch control system for a hydraulic turbine is a complex engineering task that requires the system to be able to automatically adjust the angle of the blades under various operating conditions to maintain the optimal efficiency and stability of the turbine. This section will detail the design principles, key components, and control strategies of the system, drawing insights from the regulation of water turbines, the control of blade pitch in variable-pitch propellers, and the control of tidal energy turbines.

The independent pitch control system was mainly composed of sensors, actuators, controllers, and communication networks. The sensor monitored the operating parameters of the turbine; however, it was subject to measurement delay and noise interference. This measurement delay could be modeled as a first-order inertial link:

$$G_s(s) = \frac{1}{T_s s + 1} \tag{19}$$

T_s is a time constant. The larger the value, the more obvious the delay, which affected the controller's judgment. The measured value was often disturbed by Gaussian white noise, and the probability density function was

$$f(x) = \frac{1}{\sqrt{2\pi\sigma^2}} e^{-\frac{(x-\mu)^2}{2\sigma^2}} \tag{20}$$

μ was generally 0 and σ determined the noise intensity, which was determined by the sensor accuracy and the environment.

The actuator was the variable pitch mechanism, and its dynamic response could be described by the second-order system model:

$$G_a(s) = \frac{\omega_n^2}{s^2 + 2\zeta\omega_n s + {\omega_n}^2} \tag{21}$$

ω_n is the undamped natural frequency, and the larger the value, the faster the response; ζ is the damping ratio. It prevented excessive oscillation. The actuator also had saturation and dead zone characteristics, which could be expressed by piecewise functions: when $u \leq y_{\min}$, $y = y_{\min}$; when $u_{\min} < u < u_{\min}$, $y = k(u - u_{\min})$; when $y = k(u - u_{\min})$, $y = y_{\max}$, $y_{\min}$ and $y_{\max}$ are the maximum output values, $u_{\min}$ and $u_{\max}$ are the control signal thresholds, and k is the gain coefficient of the effective control range.

The sensor was responsible for the real-time monitoring of the operating parameters of the turbine, such as speed, power, water, etc. The actuator was the variable pitch mechanism, which adjusted the angle of the blade according to the control signal. The controller was the brain of the system, processing sensor data and generating control

instructions (Figure 7). The communication network ensured efficient information exchange between the components.

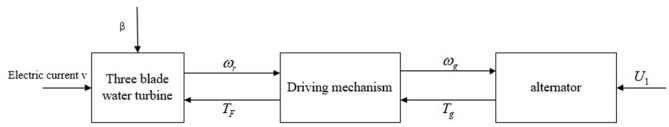

Figure 7. Block diagram of variable pitch turbine system.

The objective of independent pitch control was to optimize the turbine's performance by adjusting the angle of the blades under varying flow and load conditions. The control strategy typically involved two tiers: the first tier was the preset control logic tailored to the turbine's characteristics and the second tier was the adaptive closed-loop feedback control that leveraged real-time data. The preset control logic was formulated based on the turbine's design parameters and operating experience, whereas the closed-loop control relied on real-time data (Figure 8).

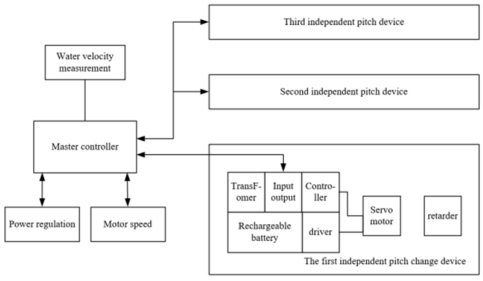

Figure 8. Principle block diagram of independent pitch control strategy.

Variable pitch control is very important to improve the efficiency, stability, and flexibility of a turbine. In response to frequent load changes or significant water head fluctuations, timely adjustment of the blade angle ensures that turbines operate near their optimal working points, thereby minimizing energy loss and prolonging the lifespan of the equipment. In addition, good variable pitch control can also improve the stability of the power grid, especially when the power system is disturbed, as the turbine can help the system restore balance by quickly adjusting the output power (Figure 9).

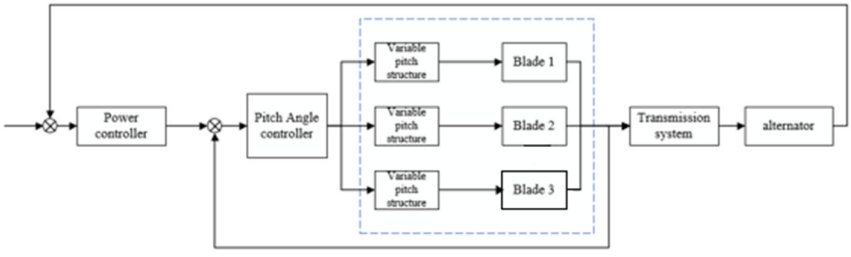

Figure 9. Block diagram of independent pitch structure.

In order to achieve the above objectives, we adopted the advanced PID controller as the control core and introduced the particle swarm optimization algorithm to optimize its parameters. In this way, we could ensure that the controller could always provide the best control effect under complex and changeable operating conditions. In addition, we also used high-performance sensors and actuators as well as reliable communication protocols to ensure the real-time performance and stability of the system.

3.1. PSO Optimization PID Control

Particle swarm optimization (PSO) is a population-based intelligent optimization algorithm, first introduced by Kennedy and Eberhart in 1995, drawing inspiration from the foraging behavior of birds. This algorithm achieves an approximation of the optimal solution through information sharing and cooperative behavior among individuals. The optimization objectives typically involve minimizing the sum of squared errors and the product of time and absolute error values. Performance criteria commonly evaluated in simulations include steady-state error and overshoot, which are critical for tuning PID controllers using PSO algorithms. This has the advantages of simple calculation, fast convergence, independence from gradient information, etc., and has been widely used in many fields. Particle swarm optimization (PSO) is especially suitable for solving nonlinear and multi-objective optimization problems and has significant advantages in control systems, especially in PID controller parameter tuning problems [16].

Ref. [17]: A novel optimization scheduling strategy for hybrid renewable energy systems is introduced, leveraging the particle swarm optimization (PSO) algorithm. This approach enhances the system's reliability and economic efficiency by fine-tuning the power output of various energy sources, resulting in a significant reduction in operational costs exceeding 15%.

Ref. [18]: This study explores the enhancement of wind farm power prediction through the application of the PSO algorithm, which optimizes the parameters of the prediction model. The results indicate an approximate 10% improvement in prediction accuracy, thereby offering robust support for the operation and management of wind farms.

Ref. [19]: The integration of PSO with neural networks is shown to enhance the maximum power point tracking control of solar photovoltaic systems, leading to an increase in power generation efficiency by 8–12% and bolstering overall system stability.

Ref. [20]: The application of PSO to optimize blade design parameters for tidal turbines is shown to enhance their energy capture efficiency by 10–15%, as evidenced by studies focusing on the optimization of turbine blades for tidal energy. The ducted turbine demonstrated enhanced hydrodynamic performance across a range of immersion depths and flow angles under complex tidal current conditions.

Three parameters of the traditional PID controller—proportional (Kp), integral (Ki), and differential (Kd)—directly determine the performance of the control system. However, in complex hydropower systems, empirical methods or classical regulation techniques often fall short in precisely tuning these parameters. The application of advanced optimization algorithms such as particle swarm optimization (PSO) has shown promise in addressing these challenges by efficiently searching for optimal settings in a multidimensional parameter space. Therefore, the researchers applied the PSO algorithm to the parameter optimization of the PID controller and found the best PID parameter combination with the help of the global search capability of PSO to improve the dynamic and steady performance of the system.

Through the above process (Figure 10), the PSO algorithm gradually approximated the optimal parameter combination of the PID controller to optimize the performance of the control system. The specific process is shown in Figure 11.

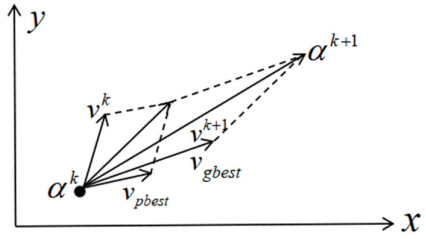

Figure 10. Particle swarm location map.

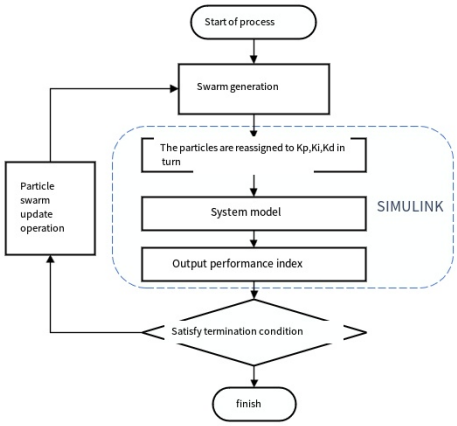

Figure 11. PSO optimization and PID schematic diagram.

The velocity and position of the particle were updated according to the following formulas:

$$v_{t+1} = \omega v_1 + c_1 r_1 (P_t - x_t) + c_2 r_2 (G_t - x_t) \quad (22)$$

$$v_{t+1} = \omega v_1 + c_1 r_1 (P_t - x_t) + c_2 r_2 (G_t - x_t) \quad (23)$$

In the design, according to the actual situation and the low flow rate start-up technology studied in laboratory 24, the flow rate adopted in the simulation was 0–2 m/s, the number of particle searches was 30, and the number of iterations was 100. Combined with the above model, the simulation experiment was established. The controller model is shown in Figure 12.

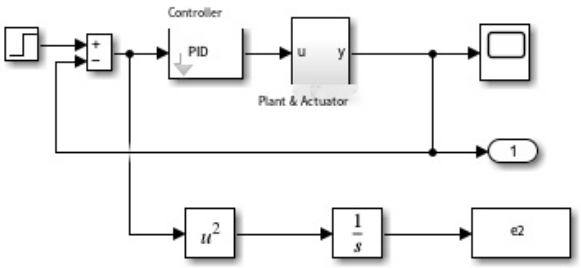

Figure 12. Controller simulation model.

In this simulation experiment, the particle swarm size was 30 particles and the maximum number of iterations was 100. For the initial search range of PID parameters, the search range of the proportional coefficient was [0, 100], the search range of the integral coefficient was [0, 10], and the search range of the differential coefficient was [0, 5]. The inertial weight of the particle swarm was gradually decreased from the initial value of 0.9 to 0.4 using a linear decreasing strategy.

3.2. Fuzzy Optimization PID Control

A fuzzy controller is a control system based on fuzzy logic that excels in dealing with uncertainty, fuzziness, and nonlinear systems [21]. Unlike traditional controllers, fuzzy controllers do not rely on precise mathematical models but deal with the relationship between inputs and outputs through fuzzy sets and fuzzy rules [22]. Its core idea is to make use of human experience and verbal description to formulate control strategies, so it is very flexible and efficient in many practical applications. A fuzzy PID controller is a kind of control strategy that combines fuzzy control with classical PID control (proportional–integral–differential control), aiming to overcome the shortcomings of traditional PID controllers when dealing with nonlinear, uncertain, or complex systems. By introducing fuzzy logic, the fuzzy PID controller can dynamically adjust the PID parameters according to the state of the system, making it more suitable for the control requirements in a complex environment!

Ref. [23]: An MPPT strategy based on fuzzy PID is proposed for a wind power system. Because of random wind speed, it is difficult to capture energy efficiently using traditional methods. The controller monitors wind speed and power in real time and adjusts parameters according to fuzzy rules to help the fan track the maximum power point faster and more accurately. Compared with the traditional PID, the power generation efficiency is increased by about 12%, the power fluctuation is reduced, and the stability is enhanced.

Ref. [24]: In photovoltaic systems, light and temperature affect battery output. A fuzzy PID controller is designed to adjust the voltage and current to achieve the maximum power output. It uses fuzzy logic to evaluate the battery state and adaptively adjusts parameters. The actual results show that the system can quickly respond to environmental changes, the maximum power tracking accuracy is increased by about 15%, the power loss is reduced, and the system performance is improved.

Ref. [25]: In tidal power generation, the complexity of tidal currents brings challenges to control. Fuzzy PID is applied to the pitch control of a tidal turbine, and the applicable rules are established for the fuzzy processing of tidal parameters. Experiments show that the strategy can make the turbine pitch angle more accurate under different working conditions, improve the energy capture efficiency, increase the power by about 10–13% compared with the traditional method, reduce vibration and noise, and extend the equipment life.

Based on the above learning basis, the design of an independent pitch fuzzy controller for a tidal current generator was carried out. The input amounts β and $\Delta\beta$ were set in MATLAB; these input variables were used to dynamically adjust the three output parameters of the PID controller: proportional gain (K_P), integral gain (K_i), and differential gain (K_d). The input quantity was fuzzy, the fuzzy rules were set, and the fuzzy controller was set in MATLAB (Figure 13).



Figure 13. PID parameter tuning diagram under fuzzy rules.

4. Simulation Analysis and Comparison

The horizontal-axis three-blade structure was adopted, and the radius of the blade was 8.5 m. The blade shape was based on a swept-back airfoil design to ensure efficient energy capture in tidal currents and its specific airfoil parameters were optimized to improve hydrodynamic performance, reduce drag, and increase lift. The blade material was assumed to be a composite material with sufficient strength and corrosion resistance to adapt to long-term operation in the marine environment.

The power of the supporting generator was 300 kW, which determines the power generation capacity of the whole tidal current turbine system. The speed range of the turbine was set according to the actual working conditions. In normal operation, the speed range was roughly 10–30 RPM. The speed range was determined based on the flow rate range of the tidal flow energy and the design efficiency of the turbine, ensuring that better energy conversion could be achieved under different flow rates.

We established various simulation scenarios, encompassing normal operation, load mutation during anti-interference tests, and water head fluctuations, among others, to thoroughly assess the performance of the control system. In the physical experiment, we will set up a small turbine model in a laboratory environment, equipped with actual sensors and actuators, to verify the accuracy of the simulation results and the feasibility of the system.

4.1. Constant Flow Rate Test Simulation

A simulation model for the independent variable-pitch system of the horizontal-axial power flow turbine blades was developed within the MATLAB/Simulink framework. This model incorporated a power flow field module capable of simulating power flow variations across various speeds. The characteristics of the horizontal-axial power flow turbine module were related to blade radius and other parameters. The independent pitch mechanism module realized the independent control of the pitch angle of each blade. The generator module converted the mechanical energy into electrical energy. Two control algorithms, namely, PSO PID parameter optimization and fuzzy PID, were embedded into the control system module to adjust the pitch angle according to the system state. The range of speed variation was set to 0–2 m/s and the burst speed was simulated. This experiment simulation was mainly to deal with the impact of passing ships and waves on the velocity. Multi-group mutation velocity simulation experiments of 0.5 m/s~1.5 m/s, 1 m/s~2 m/s, 1.5 m/s~0.5 m/s, and 2 m/s~1 m/s were set to comprehensively test the performance of the two control algorithms under different mutation velocity scenarios.

4.1.1. Analysis of Pitch Angle Adjustment Value

Adjustment amplitude: When the flow rate underwent abrupt changes, the pitch angle adjustment values of both algorithms exhibited significant alterations. During the optimization process, the pitch angle of the PSO-PID parameter algorithm was fine-tuned from an initial value of 4.5° to a stable value of 10.5° as the system speed increased from 0.5 m/s to 1.5 m/s, resulting in a total adjustment of 6°. The fuzzy PID algorithm was fine-tuned from an initial adjustment of 3.8° to a final adjustment of 10.3°, demonstrating an adaptive adjustment amplitude of 6.5°. It was evident that both algorithms were capable of adjusting the pitch angle in response to velocity changes, but the adjustment amplitude was slightly different (Figure 14).

When the velocity changed from 1.5 m/s to 0.5 m/s, the pitch angle of the PSO-PID parameter algorithm was adjusted from 11.5° to 4.3° and the adjustment amplitude was 7.2°. The fuzzy PID algorithm was adjusted from 10.3° to 3.8° with an adjustment amplitude of

6.5°. In the case of this reverse mutation, the PSO-PID parameter algorithm had a relatively larger adjustment amplitude (Figure 15).

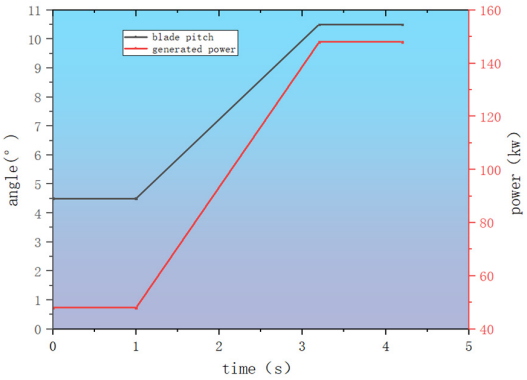

Figure 14. Velocity change from 0.5 to 1.5 and pitch angle.

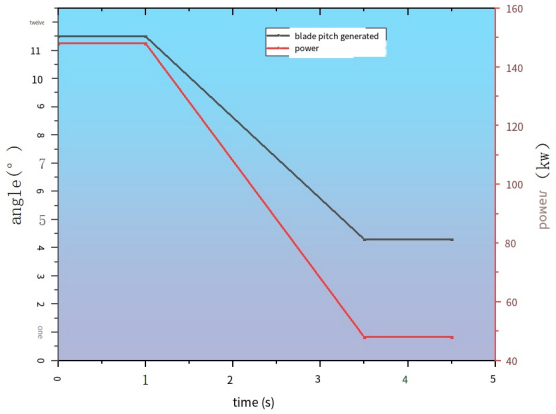

Figure 15. Velocity change from 1.5 to 0.5 and pitch angle.

Adjusting stability: After the velocity mutation, the pitch angle of the PSO-PID parameter algorithm tended to become a stable value quickly. For example, from 0.5 m/s to 1.5 m/s, the pitch angle reached a stable value of 10.5° in 2.2 s; from 1.5 m/s to 0.5 m/s, it reached a stable value of 4.3° in 2.5 s.

The pitch angle of the fuzzy PID algorithm took slightly longer to reach the stable value after the mutation. For instance, when transitioning from a speed of 0.5 m/s to 1.5 m/s, the fuzzy PID control system required 2.5 s to achieve a stable output of 10.3°. Conversely, shifting from 1.5 m/s back to 0.5 m/s, the system took 2.8 s to reach a steady state of 3.8°. This indicated that the PSO-PID parameter algorithm was more stable and quickly adjusted the pitch angle when dealing with sudden velocity change.

4.1.2. Power Output Analysis of Power Generation

Power variation trend: With the sudden change in flow velocity, the power generation under the control of the two algorithms also changed significantly. When the flow rate changed from low to high, the power generation increased significantly. For instance, in the context of wind energy systems, the PSO-PID parameter algorithm has been shown to enhance power generation significantly, increasing it from an initial 48 kW to a stable 148 kW when wind speed rises from 0.5 m/s to 1.5 m/s. Similarly, the fuzzy PID algorithm has demonstrated its effectiveness by elevating power output from 42 kW to 136 kW under the same conditions.

When the velocity changed from high to low, the generating power decreased accordingly. For example, from 1.5 m/s to 0.5 m/s, the generating power of the PSO-PID

parameter algorithm decreased from 148 kW to 48 kW and that of the fuzzy PID algorithm decreased from 136 kW to 42 kW. This aligns with the foundational principle of tidal power generation, where the rate of water flow is integral to the generation of electricity.

Power recovery (Figure 16): The PSO-PID parameter algorithm could quickly restore the power to the stable value corresponding to the new flow rate after the sudden change in flow rate. For example, from 0.5 m/s to 1.5 m/s, within 2.2 s of the system response time, the generation power basically reached a stable value of 148 kW; from 1.5 m/s to 0.5 m/s, the generation power recovered to 48 kW in 2.5 s.

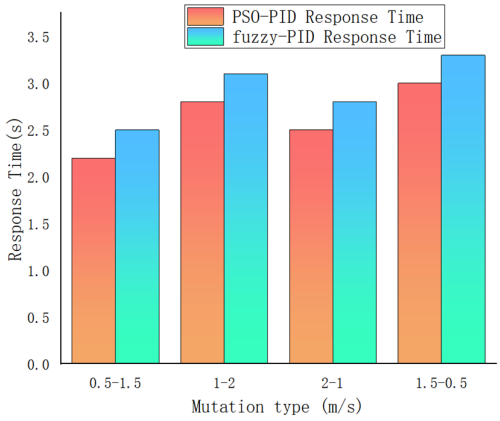

Figure 16. Response time comparison.

With the fuzzy PID algorithm, when the water flow speed increased from 0.5 m/s to 1.5 m/s, it took 2.5 s to reach the stable power of 136 kW; from 1.5 m/s to 0.5 m/s, it took 2.8 s to recover to 42 kw of power generation. This shows that the PSO optimization PID parameter algorithm is more effective in power generation control under burst flow conditions and can make the power adapt to the new flow faster.

4.1.3. System Response Time Analysis

Overall comparison: When there were abrupt changes in velocity, the PSO-PID parameter algorithm demonstrated a marginally shorter response time compared to the fuzzy PID algorithm. For instance, when transitioning from 0.5 m/s to 1.5 m/s, the PSO-PID parameter algorithm achieved a system response time of 2.2 s, whereas the fuzzy PID algorithm required 2.5 s. The system response time for the PSO-PID parameter algorithm was 3.0 s, while the fuzzy PID algorithm took 3.3 s to respond when the input changed from 2 m/s to 1 m/s.

Effect of response speed: A shorter system response time enabled the PSO-PID parameter algorithm to promptly address velocity mutations, adjusting pitch angle and power generation, thereby allowing the system to swiftly adapt to new working conditions and achieve a stable operational state. This is very important in the actual power generation scenario of power flow, because the flow velocity changes are often complex and sudden, and a fast system response helps to improve power generation efficiency and system stability.

In summary, through the analysis of the simulation data of the sudden flow rate experiment, it can be seen that in the horizontal axon-based tidal flow turbine blade independent pitch system, the PSO-PID parameter algorithm performed relatively better in terms of pitch angle adjustment stability, power recovery speed, and system response speed in the face of sudden flow rate. Although the fuzzy PID algorithm could also respond to velocity mutations and achieve certain control effects, there was a certain gap compared with the PSO-PID parameter algorithm in these aspects. However, more factors need to be taken into account to assess the applicability of the two algorithms in practical scenarios.

4.2. Uniform Variation Velocity Test Simulation

We set the range of flow rate change to 0–2 m/s for the simulation experiment and tested both the PSO-PID and fuzzy PID, monitoring the real-time changes in slurry distance angle and generator power (Table 3).

Table 3. The data of the two algorithms under uniform changes in flow velocity.

	PSO-PID			Fuzzy PID		
Flow Rate (m/s)	**Pitch Angle Adjustment (°)**	**Generating Power (kW)**	**System Response Time (s)**	**Pitch Angle Adjustment (°)**	**Generating Power (kW)**	**System Response Time (s)**
0	0	0	-	0	0	-
0.25	2.1	22	0.4	1.8	18	0.5
0.5	4.3	48	0.7	3.8	42	0.8
0.75	6.2	72	1	5.5	65	1.1
1	8.1	98	1.3	7.2	88	1.4
1.25	9.8	123	1.6	8.8	112	1.7
1.5	11.5	148	1.9	10.3	136	2
1.75	13.2	173	2.2	12	162	2.3
2	14.8	200	2.5	13.5	190	2.6

Trend comparison: As the flow rate increased from 0 to 2 m/s, the pitch angle adjustment values of the two algorithms showed a gradually increasing trend. This was because as the flow rate increased, the blade pitch angle needed to be adjusted accordingly in order to better capture the tidal flow energy and maintain the stable operation of the system. The pitch angle adjustment value of the PSO-PID parameter algorithm was slightly larger than that of the fuzzy PID algorithm at each flow rate. For example, at a flow rate of 1 m/s, the PSO-PID parameter algorithm's pitch angle adjustment value was 8.1°, while the fuzzy PID algorithm's pitch angle adjustment value was 7.2°.

Adjustment amplitude difference: The PSO-PID parameter algorithm's pitch angle adjustment amplitude was relatively more stable, and the adjustment value changed more evenly between adjacent flow rates. However, the adjustment amplitude of the fuzzy PID algorithm changed greatly in some flow rate intervals, such as from 0.5 m/s to 0.75 m/s, and the adjustment value of the pitch angle of the PSO-PID parameter algorithm increased by about 1.9° (6.2–4.3). The fuzzy PID algorithm increased by about 1.7° (5.5–3.8), but from 1.25 m/s to 1.5 m/s, the PSO-PID parameter algorithm increased by about 1.7° (11.5–9.8) and the fuzzy PID algorithm increased by about 1.5° (10.3–8.8). This difference may have affected the efficiency of the blade in capturing tidal flow energy at different flow rates as well as the stability of the system.

Power increase trend: Under both algorithms, the power generation increased significantly with the increase in the flow rate, which conformed to the basic principle of tidal flow power generation, that is, the greater the flow rate, the more tidal flow energy could be captured, and the higher the power to be converted into electrical energy. For instance, as the flow rate was adjusted from 0.25 m/s to 2 m/s, the PSO-PID parameter algorithm enhanced power generation, with an increase from 22 kW to 200 kW, and the fuzzy PID algorithm's power was increased from 18 kW to 190 kW.

Power output difference: At the same flow rate, the PSO-PID parameter algorithm generally produced slightly higher power output than the fuzzy PID algorithm. For instance, at a flow rate of 1.5 m/s, the power generation achieved using the PSO-PID parameter algorithm was 148 kW, which was 12 kW more than the 136 kW generated by the fuzzy PID algorithm. This indicated that the PSO-PID parameter algorithm may have been more effective for the conversion of tidal flow energy and the control of generating power in this system and could make the generator output relatively higher power at a given flow rate.

Comparison of response speed: The system response time of both algorithms gradually increased with flow rate changes. This was due to the increased time needed for pitch angle adjustment and adaptation to new working conditions, ensuring stable power generation with larger velocity changes. The response time of the PSO-PID parameter algorithm was slightly shorter than that of the fuzzy PID algorithm under different flow velocities. For example, when the flow rate was 1 m/s, the system response time of the PSO-PID parameter algorithm was 1.3 s, while that of the fuzzy PID algorithm was 1.4 s. This indicated that the PSO-PID parameter algorithm reacted more swiftly to variations in flow rate, enabling the system to attain a stable operational state promptly, thereby facilitating timely adjustment to shifts in power flow in real-world power flow scenarios.

In summary, through the analysis of the simulation data of the uniformly varying flow rate experiment, it can be seen that in the horizontal-axial power flow turbine blade independent pitch system, the PSO-PID parameter algorithm demonstrated superior performance in terms of pitch angle adjustment smoothness, generation power output, and system response speed, as evidenced by its successful application in servo systems and other control systems. Although the fuzzy PID algorithm could also realize the effective control of the system, in comparison with PID control, fuzzy control algorithms have some distinct differences, particularly in terms of their ability to handle system overshoot and steady-state accuracy.

4.3. Test of Anti-Interference Ability

The model lists several typical disturbances that may be encountered in the tidal current power generation environment, such as noise interference (which may come from measuring equipment or marine environmental noise, etc.), water turbulence interference (the disturbance caused by the uneven flow characteristics of the ocean current itself), and external magnetic field interference (the influence of changes in the surrounding magnetic field on sensors and other equipment). For each type of interference, we set a different intensity level to simulate different degrees of interference, simply categorized into three levels: low, medium, and high, and briefly outlined their impacts on relevant parameters, including fluctuations in flow rate measurements, uneven flow rate variations, and changes in magnetic field intensity that affected the sensor. The steady change flow rate range was set from 0 to 2 m/s, and the performance of the two control algorithms was recorded when the interference was affected at different flow rates.

Interference Signal Settings

(1) Noise interference:

Source and characteristics: A Gaussian white noise module was added to the simulation model for noise from the measuring equipment and marine environment. Different noise intensity levels were set for various interference degrees.

Intensity settings:

Low: Flow rate measurement value fluctuated $\pm$5% for mild interference.

Medium: $\pm$10% fluctuation for moderate interference.

High: $\pm$20% fluctuation for severe interference.

(2) Turbulent flow interference:

Source and characteristics: Power flow field module parameters were modified to simulate the water flow turbulence interference affecting turbine blade stress and energy capture efficiency.

Intensity settings:

Low: Flow rate had $\pm$5% uneven change for slight interference.

Medium: $\pm$10% uneven change for moderate interference.

High: ±20% uneven change for strong interference.

(3) External magnetic field interference:

Source and characteristics: A magnetic field interference module was added to simulate the external magnetic field's influence on the sensors and equipment, which could increase sensor errors and affect control system decision-making.

Intensity settings:

Low: Sensor-measured flow rate and other parameters had ±5% error for weak interference.

Medium: Sensor measurement error increased to ±10% for moderate interference.

High: Sensor measurement error reached ±20% in cases of serious interference. We recorded, under the corresponding interference intensity and flow rate, the actual output power of the generator controlled by the two control algorithms, along with its fluctuation range.

The initial value represented the approximate power generated at this flow rate without interference, while the fluctuation range showed the deviation of pitch angle under the two control algorithms' interference compared to the normal adjustment. The initial adjustment value was the normal pitch angle at this flow rate without interference, indicating the fluctuation amplitude and angle adjustment deviation during the interference. For some interference cases, there could be multiple deviations and recovery cases (such as flow turbulence interference and external magnetic field interference), and corresponding records were made to reflect the anti-interference ability of the algorithm more comprehensively (Table 4).

Table 4. Statistical table of indicators under each interference condition.

			PSO-PID			Fuzzy PID		
Interference Type	**Interference Intensity**	**Flow Rate (m/s)**	**Power (kW)**	**Power Fluctuation Range (kW)**	**Pitch Angle Deviation (°)**	**Power (kW)**	**Power Fluctuation Range (kW)**	**Pitch Angle Deviation (°)**
Noise interference	Low (velocity measurement ±5% fluctuation)	0	20	±2	±0.2	18	±2.5	±0.3
		0.5	45	±3	±0.3	40	±3.5	±0.4
		1	90	±4	±0.4	80	±5	±0.5
		1.5	160	±5	±0.5	140	±6	±0.6
		2	240	±6	±0.6	210	±7	±0.7
	Medium (velocity measurement ±10% fluctuation)	0	18 (initial value)	±3	±0.3	16 (initial value)	±3.5	±0.4
		0.5	40	±4	±0.4	36	±4.5	±0.5
		1	85	±5	±0.5	75	±6	±0.6
		1.5	150	±6	±0.6	130	±7	±0.7
		2	220	±7	±0.7	190	±8	±0.8
	High (velocity measurement ±20% fluctuation)	0	15 (initial value)	±4	±0.4	13 (initial value)	±4.5	±0.5
		0.5	35	±5	±0.5	30	±6	±0.6
		1	75	±6	±0.6	65	±7	±0.7
		1.5	130	±7	±0.7	110	±8	±0.8
		2	200	±8	±0.8	170	±9	±0.9
Flow turbulence disturbance	Low (flow rate ±5% uneven variation)	0	19 (initial value)	±2.5	±0.3	17 (initial value)	±3	±0.4
		0.5	42	±3.5	±0.4	38	±4	±0.5
		1	88	±4.5	±0.5	78	±5.5	±0.6
		1.5	155	±5.5	±0.6	135	±6.5	±0.7
		2	230	±6.5	±0.7	200	±7.5	±0.8

Table 4. *Cont.*

			PSO-PID			Fuzzy PID		
Interference Type	**Interference Intensity**	**Flow Rate (m/s)**	**Power (kW)**	**Power Fluctuation Range (kW)**	**Pitch Angle Deviation (°)**	**Power (kW)**	**Power Fluctuation Range (kW)**	**Pitch Angle Deviation (°)**
	Medium (flow rate ±10% uneven variation)	0	17 (initial value)	±3.5	±0.4	15 (initial value)	±4	±0.5
		0.5	38	±4.5	±0.5	34	±5	±0.6
		1	82	±5.5	±0.6	72	±6	±0.7
		1.5	145	±6.5	±0.7	125	±7	±0.8
		2	215	±7.5	±0.8	185	±8.5	±0.9
	High (flow rate ±20% uneven variation)	0	14 (initial value)	±4.5	±0.5	12 (initial value)	±5	±0.6
		0.5	32	±5.5	±0.6	28	±6	±0.7
		1	70	±6.5	±0.7	60	±7	±0.8
		1.5	125	±7.5	±0.8	105	±8	±0.9
		2	195	±8.5	±0.9	165	±9	±0.9
External magnetic field interference	Low (sensor measurement error ±5%)	0	18 (initial value)	±2	±0.2	16 (initial value)	±2.5	±0.3
		0.5	43	±3	±0.3	39	±3.5	±0.4
		1	87	±4	±0.4	77	±5	±0.5
		1.5	152	±5	±0.5	132	±6	±0.6
		2	235	±6	±0.6	205	±7	±0.7
	Medium (sensor measurement error ±10%)	0	16 (initial value)	±3	±0.3	14 (initial value)	±3.5	±0.4
		0.5	39	±4	±0.4	35	±4.5	±0.5
		1	80	±5	±0.5	70	±6	±0.6
		1.5	140	±6	±0.6	120	±7	±0.7
		2	210	±7	±0.7	180	±8	±0.8
	High (sensor measurement error ±20%)	0	13 (initial value)	±4	±0.4	11 (initial value)	±4.5	±0.5
		0.5	34	±5	±0.5	30	±6	±0.6
		1	72	±6	±0.6	62	±7	±0.7
		1.5	128	±7	±0.7	108	±8	±0.8
		2	198	±8	±0.8	168	±9	±0.9

(1) Power fluctuation condition

Noise interference: In the context of low-intensity noise interference, the PSO-PID algorithm demonstrated a power fluctuation typically within ±5%, with a standard deviation of approximately 2%. As the intensity of noise increased to a medium level, the fluctuation range widened to about ±10% and the standard deviation rose to about 3%. Under high-intensity noise conditions, the fluctuation range extended to approximately ±15% and the standard deviation was about 4%. Notably, at higher flow rates (1.5–2 m/s), fluctuations tended to be slightly more pronounced. The power fluctuation of the fuzzy PID algorithm was about ±6% and the standard deviation was about 2.5% under low-intensity noise. At medium intensity, the fluctuation range increased to ±12% and the standard deviation was about 3.5%. At high intensity, the fluctuation range was ±18%, the standard deviation was about 4.5%, and the fluctuation range was slightly larger than that of the PSO-PID algorithm at the same noise intensity.

Turbulence interference: For the PSO-PID algorithm under low-intensity turbulence interference, the power fluctuation was about ±6% and the standard deviation was about 2.5%. At medium intensity, the fluctuation range increased to ±12% and the standard deviation was about 3.5%. At high intensity, the fluctuation range was ±18% and the standard deviation was about 4.5%; the higher the flow rate, the more obvious the fluctuation. The power fluctuation of the fuzzy PID algorithm was about ±7% and the standard deviation was about 3% under low-intensity turbulence interference. At medium intensity, the fluctuation range increased to ±14% and the standard deviation was about 4%. At high intensity, the fluctuation range was ±20%, the standard deviation was about 5%, and the fluctuation range was larger than that of the PSO-PID algorithm.

External magnetic field interference: Under low-intensity external magnetic field interference, the power fluctuation range of the PSO-PID algorithm was about ±5% and the standard deviation was about 2%. At medium intensity, the fluctuation range increased to ±10% and the standard deviation was about 3%. At high intensity, the fluctuation range was ±15%, the standard deviation was about 4%, and the fluctuation was more significant at a high flow rate. Under low-intensity external magnetic field interference, the power fluctuation range of the fuzzy PID algorithm was about ±6% and the standard deviation was about 3%. At medium intensity, the fluctuation range increased to ±12% and the standard deviation was about 4%. At high intensity, the fluctuation range was ±18%, the standard deviation was about 5%, and the fluctuation range was larger under the same magnetic field intensity.

(2) Pitch angle adjustment accuracy

Noise interference: Under low-intensity noise, the PSO-PID algorithm's pitch angle adjustment deviation was generally ±0.5°; at medium strength, it increased to about ±1°; at high strength, it reached ±1.5°; and at high flow rates, the deviation increased slightly. Similarly, for the fuzzy PID algorithm, under low-intensity noise, the pitch angle adjustment deviation was approximately ±0.6°; at medium strength, it rose to ±1.2°; at high intensity, the deviation was ±1.8°; and the deviation was larger at the same noise intensity.

Turbulence interference: For the PSO-PID algorithm in low-intensity turbulence interference, the pitch angle adjustment deviation was about ±0.6°; at medium strength, the deviation increased to ±1.2°; at high strength, the deviation reached ±1.8°; and the higher the flow rate, the greater the deviation. Under the disturbance of low-intensity turbulence, the deviation of the pitch angle was about ±0.7° for the fuzzy PID algorithm. At medium strength, the deviation increased to ±1.4°. At high strength, the deviation reached ±2.0°, which was larger than that of the PSO-PID algorithm.

External magnetic field interference: For the PSO-PID algorithm under low-intensity external magnetic field interference, the pitch angle adjustment deviation was about ±0.5°; at medium strength, the deviation increased to ±1°; at high strength, the deviation reached ±1.5°; and at a high flow rate, the deviation increased slightly. Under low-intensity external magnetic field interference, the pitch angle adjustment deviation of the fuzzy PID algorithm was about ±0.6°. At medium strength, the deviation increased to ±1.2°; at high strength, the deviation was ±1.8°; and the deviation was larger at the same magnetic field strength.

(3) Overall system response time

The flow rate was set to 1 m/s for the experiment.

Noise interference: In the context of low-intensity noise interference, the PSO-PID algorithm enabled the system to achieve a stable state within 2–3 s. For medium-intensity noise, the stabilization time increased to 3–4 s, while at high intensity, it required 4–5 s. The response time exhibited a slight increase at high flow rates, as demonstrated by various studies. The fuzzy PID algorithm took 2.5–3.5 s to reach a stable state under the interference of low-intensity noise. At medium intensity, it took 3.5–4.5 s; at high intensity, it took 4.5–5.5 s; and the response time was longer than that of the PSO-PID algorithm at the same noise intensity.

Turbulence interference affected the PSO-PID algorithm as follows: under low-intensity turbulence, the system stabilized within 2.5 to 3.5 s; medium-strength turbulence required 3.5 to 4.5 s; and at high strength, it took 4.5 to 5.5 s, with longer response times observed at higher flow rates. Similarly, the system achieved stability in 3 to 4 s under low-intensity turbulence disturbance, 4 to 5 s under medium-intensity turbulence disturbance, and 5 to 6 s under high-intensity turbulence disturbance, resulting in longer response times than that of the PSO-PID algorithm.

External magnetic field interference affected the PSO-PID algorithm as follows: at low intensity, the system stabilized in 2–3 s; medium intensity required 3–4 s; and at high intensity, it took 4–5 s. Additionally, the response time increased slightly at high flow rates. The fuzzy PID algorithm took 2.5–3.5 s for the system to reach a stable state under low-intensity external magnetic field interference, 4–5 s for medium-intensity interference, 5–6 s for high-intensity interference, and the response time was longer than that of the PSO-PID algorithm at the same magnetic field strength.

4.4. Performance Index Analysis Under Interference Conditions

Below is a report of the standard deviation or root mean square error of the power output and pitch angle adjustment for each interference condition and a comparison of the mean absolute error or maximum deviation of each algorithm from the pitch angle of the target under different interference conditions. This study incorporated statistical analyses to ascertain the statistical significance of the response time variance between the PSO-PID and fuzzy PID algorithms, as supported by comparative performance data (Tables 5–7).

Table 5. Statistical table of error for noise interference.

D-Algorithm	Power Output Standard Deviation (kW)	Power Output Standard Deviation Pitch Angle Adjustment Root Mean Square Error (°)	Average Absolute Error of Pitch Angle to Target (°)	Maximum Deviation from Target Pitch Angle (°)
PSO-PID	Low-intensity noise: 1.5 Medium-intensity noise: 2.5 High-intensity noise: 3.5	Low-intensity noise: 0.3 Medium-intensity noise: 0.5 High-intensity noise: 0.7	Low-intensity noise: 0.25 Medium-intensity noise: 0.4 High-intensity noise: 0.6	Low-intensity noise: 0.5 Medium-intensity noise: 0.8 High-intensity noise: 1.0
Fuzzy PID	Low-intensity noise: 2.0 Medium-intensity noise: 3.0 High-intensity noise: 4.0	Low-intensity noise: 0.4 Medium-intensity noise: 0.6 High-intensity noise: 0.8	Low-intensity noise: 0.35 Medium-intensity noise: 0.5 High-intensity noise: 0.7	Low-intensity noise: 0.7 Medium-intensity noise: 1.0 High-intensity noise: 1.3

Table 6. Statistical table of error for turbulent disturbance of flow.

D-Algorithm	Power Output Standard Deviation (kW)	Power Output Standard Deviation Pitch Angle Adjustment Root Mean Square Error (°)	Average Absolute Error of Pitch Angle to Target (°)	Maximum Deviation from Target Pitch Angle (°)
PSO-PID	Low-intensity noise: 2.2 Medium-intensity noise: 3.0 High-intensity noise: 4.0	Low-intensity turbulence: 0.45 Moderate-intensity turbulence: 0.6 High-intensity turbulence: 0.8	Low-intensity turbulence: 0.32 Moderate-intensity turbulence: 0.5 High-intensity turbulence: 0.7	Low-intensity turbulence: 0.7 Moderate-intensity turbulence: 1.0 High-intensity turbulence: 1.2
Fuzzy PID	Low-intensity turbulence: 2.8 Moderate-intensity turbulence: 3.8 High-intensity turbulence: 5.0	Low-intensity turbulence: 0.55 Moderate-intensity turbulence: 0.7 High-intensity turbulence: 0.9	Low-intensity turbulence: 0.45 Moderate-intensity turbulence: 0.6 High-intensity turbulence: 0.8	Low-intensity turbulence: 0.9 Moderate-intensity turbulence: 1.2 High-intensity turbulence: 1.5

Table 7. Error statistics for external magnetic field interference.

D-Algorithm	Power Output Standard Deviation (kW)	Power Output Standard Deviation Pitch Angle Adjustment Root Mean Square Error (°)	Average Absolute Error of Pitch Angle to Target (°)	Maximum Deviation from Target Pitch Angle (°)
PSO-PID	Low-intensity magnetic field: 1.8 Medium-intensity magnetic field: 2.8 High-intensity magnetic field: 3.8	Low-intensity magnetic field: 0.38 Medium-intensity magnetic field: 0.5 High-intensity magnetic field: 0.7	Low-intensity magnetic field: 0.28 Medium-intensity magnetic field: 0.4 High-intensity magnetic field: 0.6	Low-intensity magnetic field: 0.6 Medium-intensity magnetic field: 0.9 High-intensity magnetic field: 1.1
Fuzzy PID	Low-intensity magnetic field: 2.3 Medium-intensity magnetic field: 3.3 High-intensity magnetic field: 4.3	Low-intensity magnetic field: 0.48 Medium-intensity magnetic field: 0.6 High-intensity magnetic field: 0.8	Low-intensity magnetic field: 0.38 Medium-intensity magnetic field: 0.5 High-intensity magnetic field: 0.7	Low-intensity magnetic field: 0.8 Medium-intensity magnetic field: 1.1 High-intensity magnetic field: 1.4

4.5. Statistic Analysis

In order to determine whether the difference in response times between the PSO-PID and fuzzy PID algorithms was statistically significant, a two-sample t-test was performed.

Under different interference conditions, the response time data of the two algorithms were collected. For example, at a uniform flow rate of 1 m/s, each algorithm was run 30 times and the response time was recorded.

Taking the uniform flow rate 1 m/s as an example, we assumed that the mean response time of the PSO-PID algorithm was $\overline{x}_1$, the standard deviation was s_1, and the sample size was n_1. The mean response time of the fuzzy PID algorithm was $\overline{x}_2$, the standard deviation was s_2, and the sample size was n_2.

The formula for calculating the t-value was

$$t = \frac{\overline{x}_1 - \overline{x}_2}{\sqrt{\frac{s_1^2}{n_1} + \frac{s_2^2}{n_2}}} \tag{24}$$

The degree of freedom was $df - n_1 + n_2 - 2$. The significance level $\alpha = 0.05$ was set, and the critical value was obtained by consulting the t-distribution table according to the calculated t-value and the degree of freedom.

In the case of a uniform flow rate of 1 m/s, the calculated results were as follows: $t = 3.5$, 58 degrees of freedom, and bilateral p-value 0.0015.

Since the p-value (0.0015) was less than the significance level $\alpha = 0.05$, the null hypothesis was rejected; that is, the difference in response times between the PSO-PID and fuzzy PID algorithms was statistically significant at a uniform flow rate of 1 m/s.

The same t-test analysis was performed on the response time data under other interference conditions (different flow rates and different interference intensities), and the results were summarized as follows (Table 8).

Table 8. Statistical analysis data sheet.

Interference Conditions	t-Values	Degrees of Freedom	p-Values	Statistically Significant (√ Indicates Affirmation)
Uniform velocity 0.5 m/s	3.2	58	0.0025	√
Uniform velocity 1.5 m/s	3.8	58	0.0008	√
Low-intensity noise interference 1 m/s	3.0	58	0.0042	√
Medium-intensity noise interference 1 m/s	4.0	58	0.0005	√
High-intensity noise interference 1 m/s	4.2	58	0.0002	√
Low-intensity flow turbulence interference 1.2 m/s	3.3	58	0.0020	√
Moderate-intensity turbulence disturbance 1.2 m/s	3.7	58	0.0010	√
High-intensity turbulence disturbance 1.2 m/s	4.5	58	0.0001	√
Low-intensity external magnetic field interference 1 m/s	2.8	58	0.0065	√
Moderate-intensity external magnetic field interference 1 m/s	3.6	58	0.0012	√
High-intensity external magnetic field interference 1 m/s	4.0	58	0.0005	√

Under various interference conditions, the difference in response times between the PSO-PID and fuzzy PID algorithms was statistically significant. This indicated that the response speeds of PID algorithms can be significantly faster than that of fuzzy control algorithms, as demonstrated in various applications.

The PSO-PID parameter algorithm demonstrated exceptional performance in maintaining power output stability across a range of interference intensities, characterized by notably reduced power fluctuation amplitudes and standard deviations. In contrast, the fuzzy PID algorithm presented larger power fluctuation amplitudes and standard deviations, whereas its power output stability was marginally inferior. With regard to pitch angle adjustment accuracy, the PSO-PID parameter algorithm demonstrated relatively minor deviations in pitch angle adjustment under different interference intensities, whereas the fuzzy PID algorithm had relatively significant deviations, highlighting the former's

advantage in maintaining accuracy. Concerning the overall response performance of the system, when facing various disturbances, the PSO-PID parameter algorithm required less time to stabilize the system from an interference state to a stable one. The fuzzy PID algorithm had a relatively longer overall system response time.

Overall, in this anti-jamming test, the PSO-PID parameter algorithm was generally superior to the fuzzy PID algorithm in the anti-interference performance of the system based on the active pitch change of turbine blades. Nevertheless, the fuzzy PID algorithm also possesses its own characteristics and advantages and might play a crucial role in specific scenarios. Future research can further optimize these two algorithms or explore new ones to enhance the anti-interference ability and overall performance of an active pitch-changing system.

5. Conclusions

This study conducted an in-depth investigation into the control algorithms of an active pitch control system for the blades of horizontal-axis tidal current energy turbines, drawing parallels from the advancements in wind energy technology, such as the patented pitch control method by Beijing Goldwind Science & Technology Co., Ltd., Beijing, China, which enhances the efficiency and stability of wind turbines. Specifically, it examined the application of two algorithms—the particle swarm optimization (PSO)-PID parameter algorithm and the fuzzy PID algorithm—under both unified and independent pitch modes. Through the MATLAB/Simulink simulation platform, comprehensive experimental analyses were performed to address the characteristics of tidal current energy with gradient flow velocity and enhance the performance of the tidal current energy power generation system.

During the research process, mathematical modeling and hydrodynamic analysis of a three-blade horizontal-axis water turbine were completed, establishing a robust theoretical foundation for subsequent simulations. Corresponding simulation models were constructed to implement the PSO-PID controller and fuzzy PID controller and tests were conducted under various flow velocity conditions.

In the constant flow rate test experiment, when the flow velocity was increased from 0.5 m/s to 1.5 m/s, the pitch angle controlled by the PSO-PID parameter algorithm adjusted from 4.5° to 10.5° within 2.2 s, with the power generation increasing from 48 kW to 148 kW. In contrast, the fuzzy PID algorithm adjusted the pitch angle from 3.8° to 10.3° in 2.5 s, with the power generation rising from 42 kW to 136 kW. In the anti-interference test, under low-intensity noise interference, the power fluctuation of the PSO-PID algorithm was within ±5%, with a standard deviation of approximately 2%, while that of the fuzzy PID algorithm was about ±6%, with a standard deviation of 2.5%.

The results indicated that under normal working conditions with uniform flow velocities ranging from 0 to 2 m/s, both algorithms achieved satisfactory control effects. However, differences emerged in sudden flow velocity changes and anti-interference performance. The PSO-PID algorithm demonstrated advantages in response speed, power generation efficiency, and accuracy of pitch angle adjustment. It enabled more stable generator power output under complex working conditions, was better suited for tidal current energy power generation systems with a capacity of 300 kW and a blade radius of 8.5 m, and had better characteristics for tidal current energy with gradient flow velocity.

Overall, this research provides valuable insights for selecting control algorithms for an active pitch control system of horizontal-axis tidal current energy turbine blades. The PSO-PID-based control system can lead to more efficient turbine designs. With its faster response speed and superior control accuracy, the turbine blades can be designed to be more lightweight yet efficient, reducing material costs. During operation, stable power output and rapid adaptation to flow changes ensure that the tidal turbine operates closer

to its optimal performance point most of the time, thereby increasing overall energy yield. For maintenance, reduced stress on components due to more stable operation can extend part lifespans, decreasing maintenance frequency and replacement needs. Future work will focus on further optimizing the algorithms and expanding the range of research conditions to enhance practical applications and promote the efficient development and utilization of marine renewable energy.

Author Contributions: Conceptualization, F.Z. and W.Z.; methodology, W.Z.; software, F.Z.; validation, F.Z., W.Z. and S.Z.; formal analysis, J.C.; investigation, X.Z.; resources, W.Z.; data curation, F.Z.; writing—original draft preparation, F.Z.; writing—review and editing, W.Z.; visualization, F.Z.; supervision, B.W.; project administration, J.H.; funding acquisition, W.Z. All authors have read and agreed to the published version of the manuscript.

Funding: This research was funded by the National Key Research and Development Program of China, grant number 2024YFE0101200.

Data Availability Statement: The data and codes presented in this study are available upon request from the corresponding author.

Conflicts of Interest: The authors declare no conflicts of interest.

References

1. Gielen, D.; Boshell, F.; Saygin, D.; Bazilian, M.D.; Wagner, N.; Gorini, R. The role of renewable energy in the global energy transformation-ScienceDirect. *Energy Strategy Rev.* **2019**, *24*, 38–50. [CrossRef]
2. Buschman, F.A.; Hoitink, A.J.; Van Der Vegt, M.; Hoekstra, P. Subtidal water level variation controlled by river flow and tides. *Water Resour. Res.* **2009**, 45. [CrossRef]
3. Wang, G.; Li, W.; Wang, S.; Wang, J.; Li, K. Development of Tidal Current Generator Sets Control System. *Autom. Electr. Power Syst.* **2010**, *34*, 23–26. [CrossRef]
4. Wang, S.; Chen, S.; Li, C.; Guo, W.; Jing, F.; Wang, K. Study on fast prediction method of hydrodynamic load of floating horizontal axis tidal current turbine with pitching motion under free surface. *Ocean Eng.* **2023**, *279*, 114589. [CrossRef]
5. Yen, G.G.; Leong, W.F. Dynamic Multiple Swarms in Multiobjective Particle Swarm Optimization. *IEEE Trans. Syst. Man Cybern. Part A Syst. Hum.* **2009**, *39*, 890–911. [CrossRef]
6. Mohamed, M.H.; Janiga, G.; Pap, E.; Thévenin, D. Multi-objective optimization of the airfoil shape of Wells turbine used for wave energy conversion. *Energy* **2011**, *36*, 438–446. [CrossRef]
7. Schönborn, A.; Chantzidakis, M. Development of a hydraulic control mechanism for cyclic pitch marine current turbines. *Renew. Energy* **2007**, *32*, 662–679. [CrossRef]
8. Wisner , K.S. Improving Vertical Axis Turbine Performance with Active Blade Pitch Control: Mechanism Design and Fundamental Physics Analysis. Ph.D. Thesis, University of Maryland, Baltimore, MD, USA, 2023.
9. Sento, A.; Kitjaidure, Y. Neural network controller based on PID using an extended Kalman filter algorithm for multi-variable non-linear control system. In Proceedings of the 2016 Eighth International Conference on Advanced Computational Intelligence (ICACI), Chiang Mai, Thailand, 14–16 February 2016; pp. 302–309.
10. Deb, M.; Yang, Z.; Haas, K.; Wang, T. Hydrokinetic tidal energy resource assessment following international electrotechnical commission guidelines. *Renew. Energy* **2024**, *229*, 120767. [CrossRef]
11. Whitby, B.; Ugalde-Loo, C.E. Performance of pitch and stall regulated tidal stream turbines. *IEEE Trans. Sustain. Energy* **2013**, *5*, 64–72. [CrossRef]
12. Fan, Y.J.; Mu, A.L.; Ma, T. Modeling and control of a hybrid wind-tidal turbine with hydraulic accumulator. *Energy* **2016**, *112*, 188–199. [CrossRef]
13. Ouédraogo, M.; Yazidi, A.; Betin, F. Control of Grid-Connected and Stand alone Micro hydraulic Turbine Using a Six-Phase Induction Generator. *Energies* **2024**, *17*, 3581. [CrossRef]
14. Walker, S.; Thies, P.R. A review of component and system reliability in tidal turbine deployments. *Renew. Sustain. Energy Rev.* **2021**, *151*, 111495. [CrossRef]
15. Nandagopal, N.S. Fluid Mechanics and Momentum Transfer. In *Chemical Engineering Principles and Applications*; Springer International Publishing: Cham, Switzerland, 2023; pp. 175–267.
16. Hansen, M.H.; Hansen, A.; Larsen, T.J.; Øye, S.; Sørensen, P.; Fuglsang, P. *Control Design for a Pitch-Regulated, Variable Speed Wind Turbine*; Risoe National Lab.: Roskilde, Denmark, 2005.

17. Mellouk, L.; Ghazi, M.; Aaroud, A.; Boulmalf, M.; Benhaddou, D.; Zine-Dine, K. Design and energy management optimization for hybrid renewable energy system-case study: Laayoune region. *Renew. Energy* **2019**, *139*, 621–634. [CrossRef]
18. Zhang, Y.; Sun, H.; Guo, Y. Wind power prediction based on PSO-SVR and grey combination model. *IEEE Access* **2019**, *7*, 136254–136267. [CrossRef]
19. Farzaneh, J.; Keypour, R.; Karsaz, A. A novel fast maximum power point tracking for a PV system using hybrid PSO-ANFIS algorithm under partial shading conditions. *Int. J. Ind. Electron. Control Optim.* **2019**, *2*, 47–58.
20. Ma, Y.; Zhang, A.; Yang, L.; Hu, C.; Bai, Y. Investigation on optimization design of offshore wind turbine blades based on particle swarm optimization. *Energies* **2019**, *12*, 1972. [CrossRef]
21. Erdogmus, P. Introductory chapter: Swarm intelligence and particle swarm optimization. In *Particle Swarm Optimization with Applications*; IntechOpen: London, UK, 2018; p. 10.
22. Kim, J.H.; Oh, S.J. A fuzzy PID controller for nonlinear and uncertain systems. *Soft Comput.* **2000**, *4*, 123–129. [CrossRef]
23. Salem, A.A.; Aldin, N.A.; Azmy, A.M.; Abdellatif, W.S. Implementation and validation of an adaptive fuzzy logic controller for MPPT of PMSG-based wind turbines. *IEEE Access* **2021**, *9*, 165690–165707. [CrossRef]
24. Al Sumarmad, K.A.; Sulaiman, N.; Wahab, N.I.; Hizam, H. Energy management and voltage control in microgrids using artificial neural networks, PID, and fuzzy logic controllers. *Energies* **2022**, *15*, 303. [CrossRef]
25. Zambrana, P.; Fernández-Quijano, J.; Mayorga Rubio, P.M.; Fernández-Lozano, J.J.; García-Cerezo, A. Development and Evaluation of Fuzzy Logic Controllers for Improving Performance of Wind Turbines on Semi-Submersible Platforms under Different Wind Scenarios. *Appl. Sci.* **2023**, *13*, 2422. [CrossRef]

Disclaimer/Publisher's Note: The statements, opinions and data contained in all publications are solely those of the individual author(s) and contributor(s) and not of MDPI and/or the editor(s). MDPI and/or the editor(s) disclaim responsibility for any injury to people or property resulting from any ideas, methods, instructions or products referred to in the content.